Optimum Saturation Magnetization of Superparamagnetic Iron Oxide Nanoparticles for Versatile Applications

O. Karaagac*, C. Hasirci and H. Köçkar

Balikesir University, Science & Literature Faculty, Physics Department, 10145, Cagis, Balikesir, Turkey

Received: 23.04.2024 & Accepted: 23.07.2024

Doi: 10.12693/APhysPolA.146.154 *e-mail: karaagac@balikesir.edu.tr

Due to their unique properties, magnetic nanoparticles are interesting for the fundamental study of materials science and their applications. Specifically, iron oxide nanoparticles have a wide range of applications, for example in electronic, environmental, and medical areas. In many applications, iron oxide nanoparticles with superparamagnetic behavior and high saturation magnetization are preferred since optimum magnetic properties provide better magnetic control over the nanoparticles. In the study, superparamagnetic iron oxide nanoparticles were synthesized by co-precipitation under an inert atmosphere, and the impact of most effective parameters (reaction temperature and alkali concentration) on their structural and magnetic properties was investigated. The reaction temperature was changed from 30 to 90°C, and then the alkali concentration was changed at a fixed reaction temperature. It was found that the saturation magnetization of the superparamagnetic iron oxide nanoparticles increased with the increase in reaction temperature, and the maximum saturation magnetization obtained was 67.9 emu/g with zero coercivity at 75°C. It was also observed that the particle size increased as the reaction time increased. The saturation magnetization of the superparamagnetic iron oxide nanoparticles synthesized using different alkali concentrations changed between 64.6 and 67.9 emu/g, and the particle size slightly decreased as the concentration decreased. The highest saturation magnetization (67.9 emu/g) with good crystallinity and relatively narrow size distribution was obtained at 75°C and using the highest alkali concentration. The synthesized superparamagnetic iron oxide nanoparticles may be used in a variety of potential applications, such as the removal of pollutants from water, magnetic separation, magnetic resonance imaging, etc.

topics: co-precipitation, iron oxide nanoparticles, superparamagnetism, saturation magnetization

1. Introduction

Nanotechnology has seen exponential growth in the last few decades in many areas, such as integrated electronics, biomedicine, chemistry, and engineering. Because of their special and customized qualities, nanoparticles are extremely important for research and development in a variety of fields, including electronics, environment, and medicine. Due to their unique structural, electrical, and magnetic properties, iron oxides have attracted a lot of attention recently. Many review studies [1–4] are interested in presenting the synthesis and characterization techniques of iron oxide nanoparticles as well as their properties and applications. Despite being investigated for many years, uncoated and coated/functionalized forms of iron oxide nanoparticles are still attracting attention.

Iron oxide nanoparticles are one of the types of the magnetic nanoparticles that have a wide range of application areas, such as electronics [5, 6], sensors [7, 8], ferrofluids [9], environmental applications [10, 11], and medicine [12–17]. All applications have specific requirements for the effective use of magnetic nanoparticles. However, it can be said that the most important requirement is a superparamagnetic character with a high saturation magnetization, M_s, since the requirements in applications of magnetic nanoparticles mainly focus on these properties.

In an electronic application in [6], magnetic ink composed of superparamagnetic nanoparticles with an improved M_s compared to its commercial equivalent was obtained and investigated for fully printed tunable radio frequency devices. Iron oxide nanoparticles were also studied for the removal of metal ions [18] and fluoride [19] from water samples. Iron oxides and magnetic composites give the opportunity for magnetic separation in wastewater treatment; however, the applications of magnetic nanoparticles are not limited to only water samples but also extend to agricultural, biological, and food samples [20]. The

oxidized zero-valent iron core–shell structure, magnetite (Fe_3O_4), maghemite (γ-Fe_2O_3), and hematite (α-Fe_2O_3) are commonly employed in heterogeneous catalysis procedures and have been deemed as appealing substitutes for the remediation of organic compound-contaminated wastewaters and soils [21]. Besides, magnetic nanoparticles can also be functionalized to extend the application potentials. In [22], surface active amine-functionalized silica-coated iron oxide nanoparticles were prepared by a two-step synthesis process involving co-precipitation. The synthesized nanoparticles were used for magnetically recyclable adsorption of aqueous carbon dioxide (CO_2). In the study, it was shown that the nanoparticles are highly dispersed in the absence of a magnetic field, and the magnetic nanoparticles exhibited a faster separation of the adsorbent nanoparticles from their dispersion using a simple, easily accessible permanent magnet for multiple adsorption–desorption and recycling applications. Thus, magnetic control over these nanoparticles is very important for magnetic separation. Superparamagnetic character and high M_s provide an advantage for separation applications. Furthermore, Fe_3O_4 and γ-Fe_2O_3 forms of iron oxides have been commonly used in biomedicine because of their high M_s and superparamagnetic character below a certain particle size [21]. Medical applications in diagnosis and treatment are diverse and include magnetic resonance imaging (MRI), drug and gene delivery, biosensor applications, and magnetic hyperthermia [12–17]. Iron oxide nanoparticles are approved magnetic materials for human use [23, 24]. Moreover, even without surface modifications for targeting, superparamagnetic iron oxide nanoparticles (SPIONs) offer good in vivo biodistribution. The SPIONs can be guided by an external magnetic field, and this controlled mobilization enables the delivery of particles to the desired target area and fixes them at the local site so that the side effects and dosage limitations can be overcome [25]. In study [16], citrate-coated SPIONs were synthesized by co-precipitation, and monodisperse SPIONs were obtained by centrifugation. The nanoparticles were analyzed for their MRI, magnetic particle imaging (MPI), and magnetic fluid hyperthermia (MFH) performances in accordance with the clinically used iron oxide nanoparticles. Magnetic properties of the synthesized nanoparticles were also investigated, and it was found that the M_s values of the nanoparticles were higher than those of the clinically used ones. It was highlighted that both MRI and MPI rely on the use of magnetic nanoparticles with strong M_s, high magnetic susceptibility, and no coercivity ($H_c = 0$). As for MFH, it was said that in order to obtain efficient heating under an alternating magnetic field, M_s should be as high as possible [16, 26]. For specific applications like MRI, MPI, and bioseparation, it can be said that SPIONs with high M_s are among the most preferred candidates [16, 25, 27].

There are a variety of ways to produce SPIONs [1–3, 28]. One of many synthesis techniques is co-precipitation. It is a simple, fast, and cost-effective method to synthesize iron oxide nanoparticles [28]. It is frequently employed in the production of iron oxide nanoparticles with tailored sizes and magnetic characteristics. Through the addition of an alkali in an inert atmosphere at room temperature or above, nanoparticles are created from aqueous solutions using this technique. With a stoichiometric ratio of $Fe^{+2}/Fe^{+3} = 1/2$ in a non-oxidizing atmosphere, full precipitation is predicted to occur in a pH range of 8–14 [25]. However, in order to obtain nanoparticles with desired properties, it should be taken into account that the particle size and magnetic properties of the final product are affected by the reaction parameters [29]. The size and shape of the iron oxide nanoparticles may depend on the type of salts and alkali sources used, the ratio of ferric and ferrous ions, the pH of the medium, the reaction temperature, the ionic strength, the stirring rate, and pouring speed of alkali solution [30–32]. Fe_3O_4 nanoparticles were prepared by co-precipitation with different concentrations of ammonia, and it was observed that the size of the nanoparticles strongly depended on the concentration of ammonia, and the crystallite size decreased from 11.8 to 6.6 nm with increasing ammonia concentration [31]. In another study [32], iron oxide nanoparticles were co-precipitated by changing the alkali source and reaction temperature. The crystallite size decreased when the temperature increased from 50 to 70°C. It was also determined that nanoparticles with a synthesis temperature of 70°C resulted in a smaller crystallite size for all alkali solutions, especially for the strong ones (potassium hydroxide and sodium hydroxide). Furthermore, the M_s values of nanoparticles may also be affected by the reaction parameters — directly or through the composition and particle size effect [1, 25, 29, 33–35]. In [34], the effect of ammonium hydroxide concentration on the composition, morphology, and magnetic properties of co-precipitated iron oxide nanoparticles was studied. It was observed that the alkali concentration played a significant role in the morphology and composition of the nanoparticle. Samples synthesized using low alkali concentration showed a typical paramagnetic curve, thus proving the low volume fraction of magnetically ordered phases. At higher concentrations, the relationship between composition and magnetization was clearly observed, as the magnetization M_s of the samples increased proportionally with increasing alkali concentration. In another study [35], the structural and magnetic properties of iron oxide nanoparticles were investigated in relation to the initial concentration of iron salts. It was revealed that a decrease in the concentration of iron salts in the initial solution led to the formation of an amorphous phase and, thus, a tendency to decrease the value of M_s.

In addition to the co-precipitation of uncoated iron oxide nanoparticles, in many studies, coated/functionalized nanoparticles are synthesized by two-step synthesis involving co-precipitation, and iron oxide nanoparticles obtained in the first step serve as a core that provides magnetic properties [15, 16, 22, 36–38]. In [36], polyethylene glycol (PEG)-coated Fe_3O_4 nanoparticles were obtained by a two-step synthesis. After synthesizing Fe_3O_4 nanoparticles, PEG solution was slowly added, and stirring was continued at 400 and 700 rpm to obtain PEG-coated nanoparticles. In [15], Fe_3O_4 nanoparticles were synthesized in order to be used as an electrochemical biosensor for glucose detection. In the study, Fe_3O_4 nanoparticles were synthesized through co-precipitation, and polyvinyl alcohol–Fe_3O_4 nanocomposite was prepared by dispersing synthesized nanoparticles in the polyvinyl alcohol (PVA) solution as a second step of the process. In another study [37], PVA-stabilized iron oxide nanoparticles were prepared using an ultrasonic-assisted co-precipitation process. Iron oxide nanoparticles were obtained by co-precipitation, and then the nanoparticles were sonicated with PVA by using an ultrasonic bath to obtain the final nanoparticles. It was observed that M_s of PVA-stabilized iron oxide nanoparticles (45.08 emu/g) was enhanced compared to uncoated iron oxide nanoparticles (41.93 emu/g). On the other hand [38], Fe_3O_4 nanoparticles were prepared by co-precipitation in the first step, and for the modification, the suspension of Fe_3O_4 nanoparticles and Poly-L-Lysine solution was sonicated in the ice bath. The saturation magnetization M_s of synthesized Fe_3O_4 nanoparticles decreased drastically with the modification. Citrate-coated SPIONs were also obtained by a two-step synthesis procedure [16]. First, SPIONs were obtained by co-precipitation, and after adding a certain amount of hydrochloric acid and sonication, citrate solution was added and stirred for 2 h. The values of M_s of the synthesized samples were found to be higher than those of M_s of commercially available nanoparticles. It was concluded that the nanoparticles with high M_s were preferred in all applications. Finally, nanoparticles were investigated for MRI, MPI, and MFH applications. In [22], surface active amine-functionalized silica-coated magnetic iron oxide nanoparticles (Fe_3O_4/SiO_2–NH_2) were prepared by a simple two-step process for adsorbing CO_2 gas from an aqueous medium. In the absence of an external magnetic field, the Fe_3O_4/SiO_2-NH_2 particles are fully dispersible in aqueous medium. However, in the presence of a permanent magnet, the nanoparticles were completely separated from their aqueous dispersion. As stated in the study, magnetic iron oxide nanoparticles ensure suitable magnetism that allows for relatively easier and faster separation of the adsorbent materials from the dispersion medium via magnetic attraction by using a simple permanent magnet.

The magnetic properties of the core nanoparticles obtained in the first step are extremely important for coated or functionalized nanoparticles. Thus, the aim of this study is to improve the saturation magnetization M_s of SPIONs since optimum magnetic properties may provide better magnetic control over the SPIONs in applications. It should be pointed out that SPIONs can be used as uncoated nanoparticles as well as the core material of the coated/functionalized nanoparticles. In all cases, it is therefore important to obtain high M_s values of SPIONs in the experimental process. With the optimization of the synthesis parameters of co-precipitation, the SPIONs with desired properties can be obtained for potential applications such as magnetic separation, water purification, etc. Thus, in this study, the most effective parameters (reaction temperature and alkali concentration) of co-precipitation were investigated, and the SPIONs with optimum M_s were obtained.

2. Experimental details

Iron oxide nanoparticles were synthesized by co-precipitation technique. $FeCl_2 \cdot 4H_2O$ (Merck, $> 99\%$), $FeCl_3 \cdot 6H_2O$ (Sigma-Aldrich, $> 99\%$), and NH_4OH (Merck, 25% of ammonia) were used for the synthesis. The molar ratio of Fe^{2+}/Fe^{3+} was kept at $\frac{1}{2}$, and N_2 was used during the synthesis. To obtain iron salt solution, 0.2479 g $FeCl_2 \cdot 4H_2O$ and 0.6758 g $FeCl_3 \cdot 6H_2O$ were dissolved in 25 ml deionized water. Then, 25 ml of NH_4OH was poured quickly to obtain an iron oxide nanoparticles. In order to investigate the effects of reaction parameters and to obtain iron oxide nanoparticles with optimum properties, temperature and alkali concentration were changed accordingly. The reaction temperature was varied between 30 and 90°C, and diluted NH_4OH solutions with different concentrations, from 2.6 to 13.3 M, were used as an alkali source. The reaction was performed at 1000 rpm, and reaction time was fixed at 30 min. After the reaction, the sample was placed on the neodymium magnet, the nanoparticles were magnetically separated, and the supernatant was removed. The precipitate was washed several times with deionized water, separated magnetically in the same way, and dried in an oven for characterization. Dispersions of the nanoparticles were obtained by using the procedure described in [39].

Structural characterizations were made using the X-ray diffraction technique (XRD, PANalytical X'Pert Pro) and Fourier transform infrared spectroscopy (FTIR, PerkinElmer Spectrum Two). XRD measurements were performed between $2\theta = 20$–$80°$ by using Cu K_α ($\lambda = 0.15406$ nm) radiation. KBr pellets were used for FTIR analysis, and the scan was performed between 400–4000 cm^{-1}. A transmission electron microscope (TEM, FEI

Tecnai G2 F30 model) was used for the determination of particle shape and size. A drop of the diluted dispersion was placed onto the grid and allowed to air-dry before the imaging. An accelerating voltage of 200 kV was used, and particle sizes were calculated for over 200 nanoparticles from the TEM images by using ImageJ software. A vibrating sample magnetometer (VSM, ADE Technologies EV9) was used to investigate the magnetic properties of the nanoparticles. The magnetic field was applied up to ±20 kOe (1 Oe intervals) at room temperature.

3. Results and discussion

Iron oxide nanoparticles were synthesized by co-precipitation under an inert atmosphere to obtain the optimum M_s for possible use in applications [1–4]. Primarily, the effective parameters in our experimental setup were investigated. For this purpose, reaction temperature, stirring rate, reaction time, and alkali concentration were changed, and the effects of these parameters on the structural and magnetic properties of the nanoparticles were studied separately. According to the findings, the two most effective parameters were selected and extensively studied in order to obtain high M_s for the nanoparticles. First, the effect of reaction temperature on the properties of the nanoparticles was investigated as the alkali concentration was fixed at a maximum value (13.3 M). In the second stage, the alkali concentration was changed at a fixed reaction temperature (75°C).

The XRD patterns of samples synthesized at 30°C (T30) and 75°C (T75) are given with the peaks of magnetite in Fig. 1. In the XRD pattern of the nanoparticles synthesized at 30°C, the peaks of (220), (311), (511), and (440) planes are seen at around $2\theta \approx 30°, 35°, 57°$, and 63°, respectively. These peaks can be attributed to magnetite according to the JCPDS card no. 019-0629 (see Fig. 1). In the XRD pattern of T75, the (400) peak of magnetite at around $2\theta \approx 43°$ is also observed aside from the peaks labeled in the pattern of T30. Besides, two weak peaks are seen at $2\theta \approx 53°$ and 74° and can be labeled as (422) and (533), respectively. The pattern of T30 only shows the most intense four peaks of magnetite, however, the pattern of T75 includes three other peaks of magnetite aside from the ones observed in the pattern of T30. The crystallite size of the nanoparticles was estimated by using the Scherrer equation [40]. The wavelength of Cu K_α (1.5406 nm) and the constant $K = 0.9$ were used for the calculation. Two-theta and full width at half maximum (FWHM) values of each peak are given with their respective estimated particle size in Table I. For sample T30, particle sizes are estimated to be around 7–8 nm for three peaks and 15.4 nm for the (511) peak. For sample T75, however, particle sizes estimated for four peaks are very close to each other and around 11 nm, and a particle size of 7.5 nm for the (311) peak was also calculated. The average crystallite size, d_{XRD}, of the nanoparticles was estimated using the most intense three peaks of each sample. The average d_{XRD} of samples T30 and T75 are calculated to be 7.7 and 9.4 nm, respectively (Table II). It is observed that the mean particle size of iron oxide nanoparticles increases with the increase in reaction temperature.

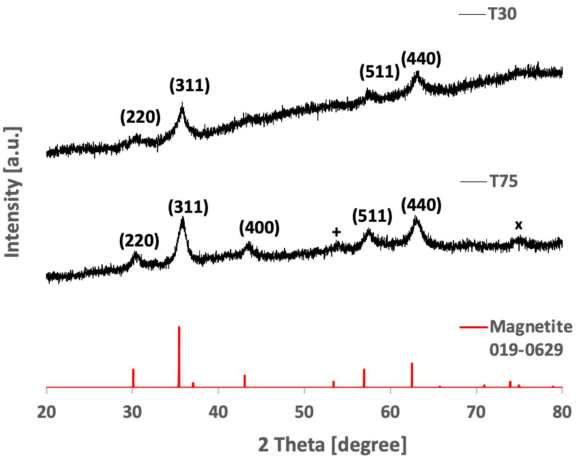

Fig. 1. XRD patterns of magnetite (JCPDS 019-0629) and the samples synthesized at 30°C (T30) and 75°C (T75). (Note that "+" represents (422) and "x" represents (533) peaks).

TABLE I

XRD data and particle sizes of the nanoparticles (T30 and T75).

Sample	2θ [°]	FWHM	d [nm]
T30	30.4768	1.0479	8.0
	35.7934	0.9800	8.7
	57.3271	0.5987	15.4
	63.1307	1.3451	7.1
T75	30.2656	0.7428	11.3
	35.8460	1.1328	7.5
	43.5009	0.7764	11.2
	57.4322	0.8216	11.3
	62.8550	1.0226	11.1

For further structural characterization, FTIR was used. The spectrum of the nanoparticles synthesized at different reaction temperatures is given in 1200–400 cm^{-1} region in Fig. 2. All samples show similar spectrum. There are transmittance peaks/bands at around 430, 560–580, and around 625 cm^{-1}. It is stated that these peaks indicate the Fe–O stretching vibration in the tetrahedral site [41]. It is also said that the peaks at 400 and 580 cm^{-1} correspond to magnetite, whereas the peaks at 460, 560, 580, and 620 cm^{-1} are related to maghemite [42]. Thus, the samples synthesized at different reaction temperatures may include both magnetite and

TABLE II

Particle sizes and magnetic properties of the nanoparticles synthesized at different temperatures.

Sample	Reaction temperature [°C]	Alkali concentration [M]*	Particle size [nm]		Magnetic properties	
			d_{XRD}	d_{TEM}	M_s [emu/g]	H_s [Oe]
T30	30	13.3	7.7	6.2 ± 1.2	54.0	13055
T45	45		–	–	60.5	11758
T60	60		–	–	63.7	11828
T75	75		9.4	10.1 ± 2.2	67.9	11075
T90	90		–	–	66.2	11628

*The prepared alkali solution is 25 ml.

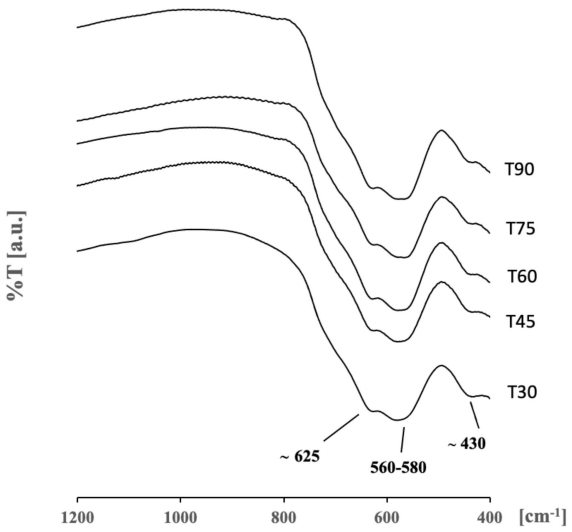

Fig. 2. FTIR spectrum of the samples synthesized at different reaction temperatures (T30 at 30°C, T45 at 45°C, T60 at 60°C, T75 at 75°C, T90 at 90°C).

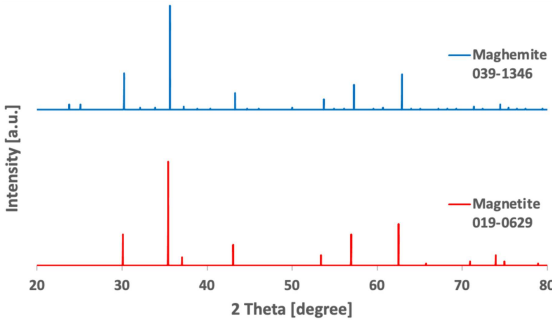

Fig. 3. XRD patterns of magnetite (JCPDS 019-0629) and maghemite (JCPDS 039-1346).

maghemite. In the XRD analysis, the peaks of magnetite are also given as a reference in Fig. 1. However, the most intense peaks observed in the XRD patterns of magnetite (JCPDS 019-0629) and maghemite (JCPDS 039-1346) are similar, with a slightly higher Bragg angle for maghemite (see Fig. 3). It is hard to distinguish them by XRD patterns. According to XRD and FTIR analysis, the synthesized nanoparticles may include magnetite and maghemite and can be called iron oxide.

In the case of reaction temperature, transmission electron microscope (TEM) images of sample T30 are given in Fig. 4 with the histogram as an inset in Fig. 4b. The images of sample T75 are also given in Fig. 5 with a high-resolution image at the 5 nm scale in Fig. 5c. The physical particle sizes, d_{TEM}, of T30 and T75 were obtained from the images and are given in Table II as 6.2 ± 1.2 and 10.1 ± 2.2 nm, respectively. Particle size is found to increase as the reaction temperature increases. From the high-resolution TEM (HRTEM) image of T75 in Fig. 5c, interplanar spacing d of the selected nanoparticles was measured and shown in the image. The measured values of $d_{(311)} = 0.25$ nm indicate the existence of iron oxide nanoparticles with (311) direction (see Fig. 5c). The result is consistent with the XRD analysis of the sample T75. In [32], iron oxide nanoparticles were co-precipitated by changing the reaction temperature. In contrast to our study, it was shown in study [32] that the particle size of the nanoparticles obtained using NH_4OH gradually decreased from 11 to 7 nm with the increase in temperature from 25 to 70°C.

Magnetic properties of the nanoparticles synthesized at different reaction temperatures were measured, and the magnetization curves are given in Fig. 6 with an inset showing the curves at ±200 Oe. Magnetization curves have no remanent magnetization, $M_r = 0$, and no coercivity, $H_c = 0$, indicating the nanoparticles are superparamagnetic. The saturation magnetization, M_s, of the nanoparticles gradually increases from 54.0 to 67.9 emu/g with the increase in reaction temperature from 30 to 75°C, and then it decreases to 66.2 emu/g as the temperature further increases to 90°C. The saturation field, H_s, decreases from 13055 to 11075 Oe as the reaction temperature increases from 30 to 75°C, and the measured H_s increases to 11628 Oe at the reaction temperature of 90°C. The values of M_s and H_s of the nanoparticles are given in Table II. Maximum M_s is obtained for the T75 sample with a minimum H_s value. It can be said that the optimum reaction temperature to obtain SPIONs with

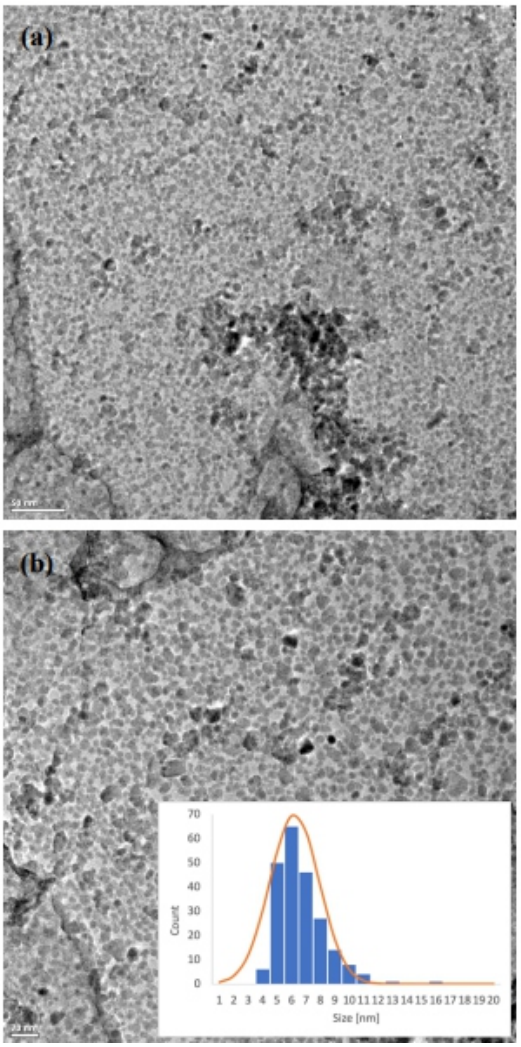

Fig. 4. TEM images of the nanoparticles synthesized at 30°C at the (a) 50 nm scale and (b) 20 nm scale. (Inset in (b) shows the histogram of T30).

high M_s (67.9 emu/g) is 75°C for our experimental setup. It is indicated in [25, 43, 44] that in the preparation of Fe_3O_4, precipitation at temperatures below 60°C produces an amorphous hydrated oxyhydroxide that can be converted to Fe_2O_3, while higher reaction temperatures (over 80°C) favor the formation of Fe_3O_4. Although it is hard to distinguish the difference in the XRD patterns under study, the increase in the M_s value with the increase in reaction temperature and reaching the highest values at 75 and 90°C may be a sign that the dominant phase is Fe_3O_4 because it is known that the bulk M_s value of Fe_3O_4 is higher than the bulk M_s value of Fe_2O_3 [45]. However, the phase difference cannot be presented as the sole cause of the change in magnetic results, and the relation between particle size and M_s should also be taken into account. It is seen that the M_s values from hysteresis curves increase as the particle size increases, as obtained from XRD and TEM analysis.

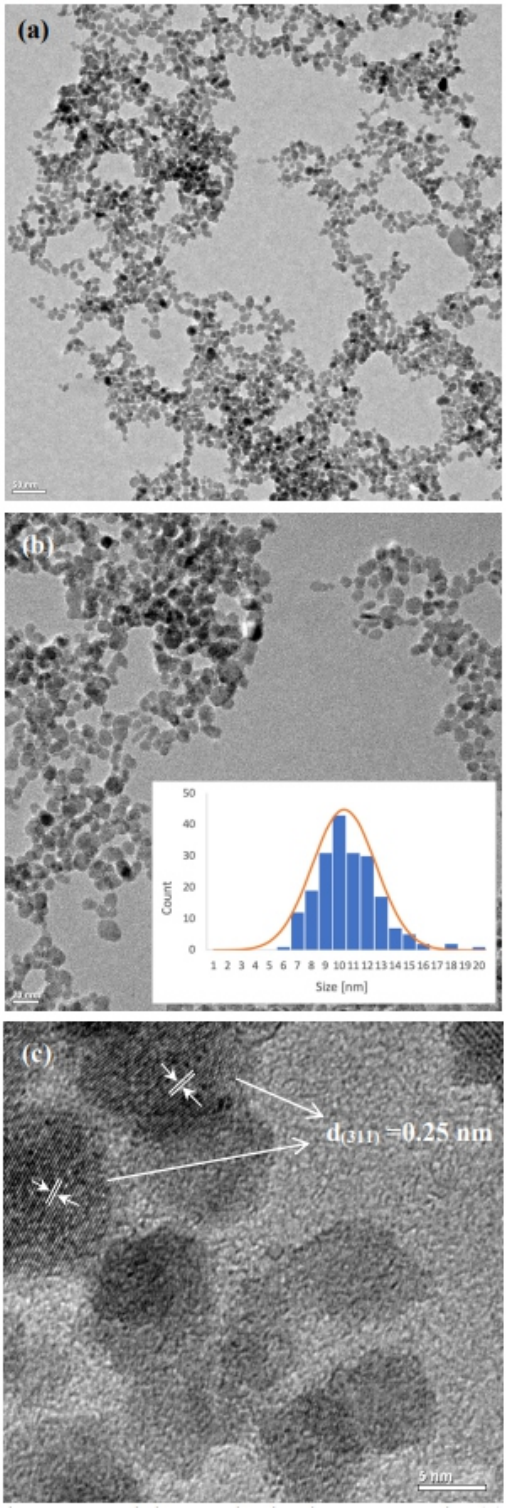

Fig. 5. TEM images of the nanoparticles synthesized at 75°C at the (a) 50 nm scale, (b) 20 nm scale, and (c) 5 nm scale (Inset in (b) shows the histogram of T75).

In the second stage, the alkali concentration was changed at a fixed reaction temperature of 75°C. The alkali concentration used in co-precipitation was changed from 13.3 to 2.6 M. The XRD patterns

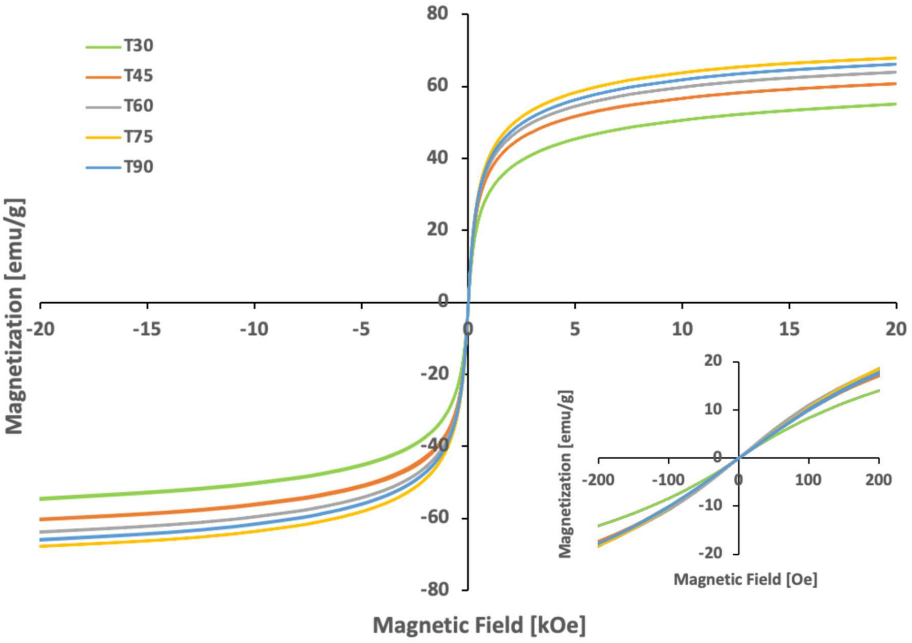

Fig. 6. Magnetization curves of the samples synthesized at different temperatures. (Inset shows the curves at ±200 Oe).

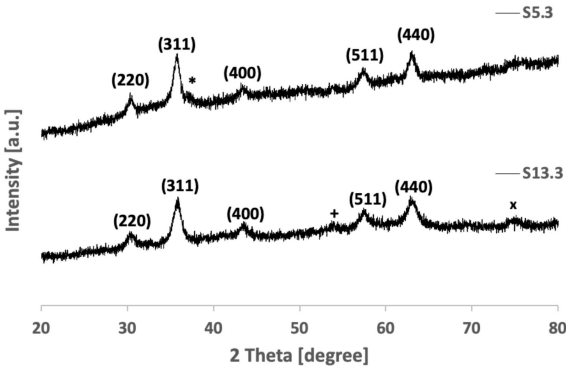

Fig. 7. XRD patterns of the samples synthesized by using 13.3 M (S13.3) and 5.3 M (S5.3) NH_4OH (Note that "$*$" represents (222), "$+$" represents (422), and "**x**" represents (533) peaks).

TABLE III

XRD data and particle sizes of the nanoparticles (S13.3 and S5.3).

Sample	2θ [°]	FWHM	d [nm]
S13.3 (T75)	30.2656	0.7428	11.3
	35.8460	1.1328	7.5
	43.5009	0.7764	11.2
	57.4322	0.8216	11.3
	62.8550	1.0226	11.1
S5.3	30.3181	0.7632	11.0
	35.7934	0.9214	9.3
	43.1858	0.3401	25.6
	57.3665	1.0351	8.9
	63.0650	0.9981	9.5

of the samples synthesized using alkali concentrations of 13.3 M and 5.3 M are given in Fig. 7 (samples are labeled S13.3 and S5.3, respectively). The sample S13.3 is the same sample as T75, and the XRD pattern of T75 is reproduced in Fig. 7 for comparison with S5.3. In the pattern of S13.3, characteristic (220), (311), (400), (511), and (440) peaks of iron oxide are clearly observed at around $2\theta \approx 30°, 35°, 43°, 57°$, and 63°, respectively. The peaks with low intensities are seen at $2\theta \approx 53°$ and 74° (labeled in the pattern by "$+$" and "**x**") and attributed to (422) and (533) planes of iron oxide, respectively. In the pattern of S5.3, (220), (311), (400), (511), and (440), peaks of iron oxide are observed. Unlike S13.3, a weak peak around $2\theta \approx 37°$ appeared in the pattern of S5.3. This peak can be labeled as (222) according to JCPDS 019-0629 and JCPDS 039-1346 cards. Two-theta and FWHM values of each peak are given with their respective estimated particle sizes in Table III. As stated before, particle sizes are very close to 11 nm for four peaks, and a different size of 7.5 nm is estimated for the (311) peak in the pattern of sample S13.3 (T75). However, the sizes vary between 8.9 and 11 nm for sample S5.3. Also, a notably different value (25.6 nm) is observed for the (400) peak. Note that d_{XRD} was estimated from the three most intense peaks in each pattern and is presented in Table IV. As can be seen, d_{XRD} characterizing the samples S13.3 and S5.3 is 9.4 and 9.3 nm,

TABLE IV

Particle sizes and magnetic properties of the nanoparticles synthesized at different alkali concentrations.

Sample	Reaction temperature [°C]	Alkali concentration [M]*	Particle size [nm]		Magnetic properties	
			d_{XRD}	d_{TEM}	M_s [emu/g]	H_s [Oe]
S13.3	75	13.3	9.4	10.1 ± 2.2	67.9	11075
S10.6		10.6	–	–	65.0	11896
S8.0		8.0	–	–	64.6	11830
S5.3		5.3	9.3	8.8 ± 2.5	66.9	11472
S2.6		2.6	–	–	66.7	10977

*The prepared solution is 25 ml.

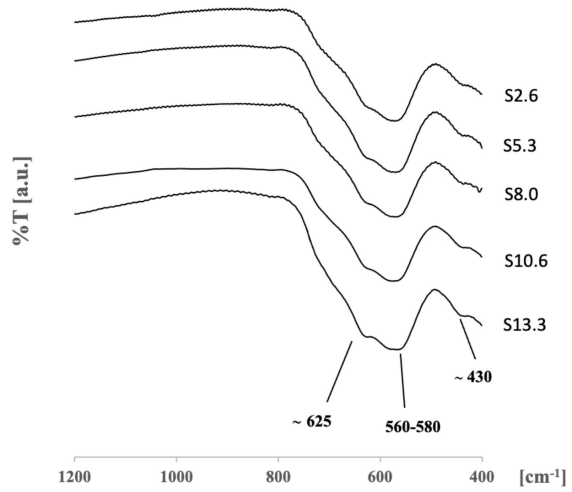

Fig. 8. FTIR spectrum of the samples synthesized at different alkali concentrations.

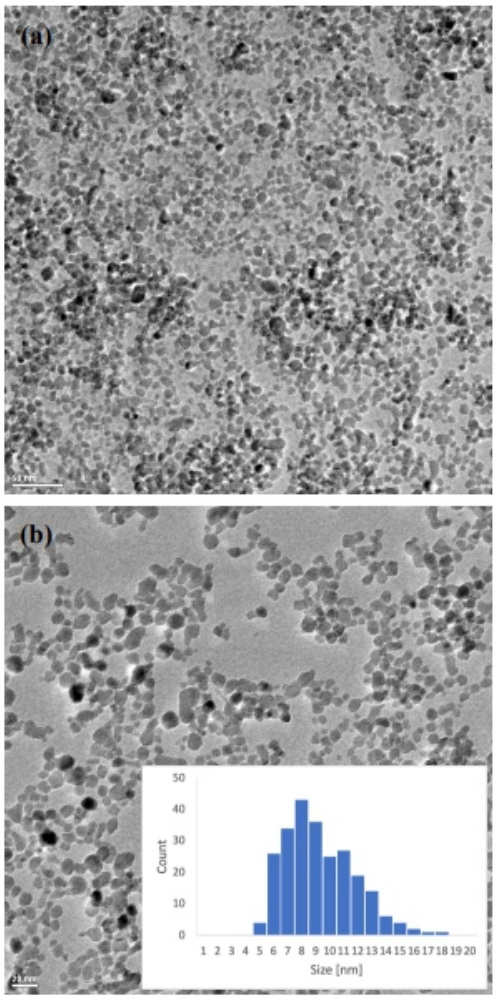

Fig. 9. TEM images of the nanoparticles synthesized using 5.3 M NH_4OH; (a) 50 nm scale and (b) 20 nm scale. (Inset in (b) shows the histogram of S5.3).

respectively. In [31], it was found that the crystallite size decreased linearly from 11.8 to 6.6 nm with the increase in ammonia concentration. In that study, Fe_3O_4 nanoparticles were prepared by co-precipitation with four different concentrations of ammonia, however, a mixture of solutions of iron salts was added dropwise to the alkali solution under vigorous stirring, which was different from our study.

The FTIR spectra of the samples synthesized at different alkali concentrations are given in Fig. 8. The spectra of all samples show similar bands. The bands observed in the spectrum are around 430 and 560–580 cm^{-1}, and the shoulder peak at around 625 cm^{-1} is present. The observed peaks/bands confirm that all samples are iron oxides [41].

The TEM images of sample S5.3 are given in Fig. 9 with the histogram. The images of S13.3 (T75) have been given in Fig. 5. From TEM images, d_{TEM} of S13.3 and S5.3 are calculated to be 10.1 ± 2.2 and 8.8 ± 2.5 nm, respectively (see Table IV). The histogram in Fig. 9b shows a slightly bimodal distribution of the nanoparticles synthesized at 5.3 M alkali concentration. Although particle sizes are concentrated around 8 nm, a number of nanoparticles with a particle size of ~11 nm can be observed. The particle size distribution of S13.3 (T75) (see the histogram in Fig. 5b) can be considered more favorable than that of S5.3. It is stated in [25, 46] that if the alkali sources are poured as quickly as possible into the ionic solution under vigorous stirring, a black colloid can be obtained,

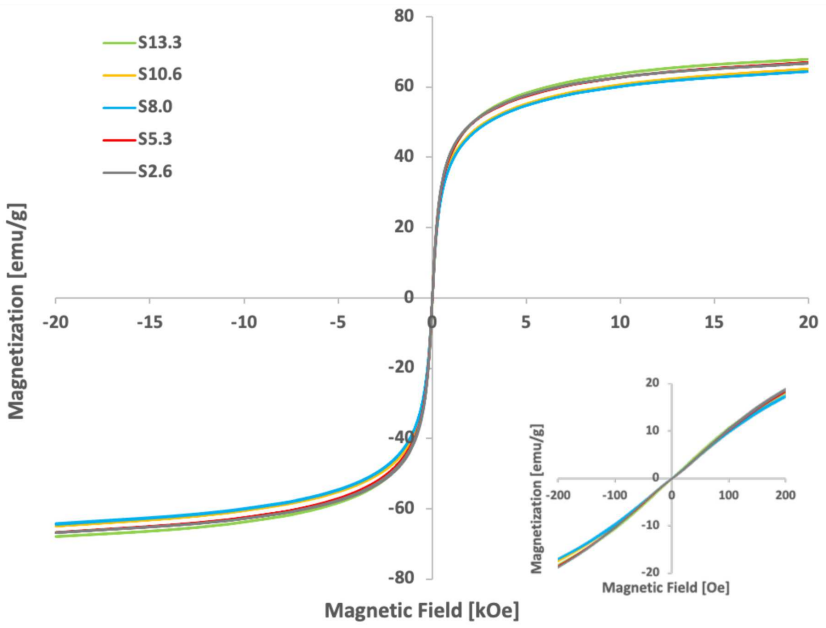

Fig. 10. Magnetization curves of the samples synthesized at different alkali concentrations. (Inset shows the curves at ±200 Oe).

but the size distribution becomes wide. Although a higher alkali concentration is used for the synthesis of S13.3, the size distribution determined from TEM images is favorable compared to that of S5.3.

Magnetization curves of the nanoparticles synthesized using different alkali concentrations are given in Fig. 10. Also, an inset is given to show the curves of the samples between −200 and +200 Oe. Magnetic data is presented in Table IV. According to the magnetic measurements at room temperature, the nanoparticles are superparamagnetic without M_r and H_c. The saturation magnetization M_s of the nanoparticles changes between 64.6 and 67.9 emu/g with the variation of alkali concentration between 2.6 and 13.3 M. Also, the H_s value changes from 10977 to 11896 Oe as the alkali concentration changes between 2.6 and 13.3 M. The highest M_s of SPIONs for the alkali concentration parameter was obtained for sample S13.3 as 67.9 emu/g.

The structural and magnetic properties of iron oxide nanoparticles were investigated according to the initial concentration of iron salts in [35]. The maximum M_s of iron oxide nanoparticles synthesized by co-precipitation was 39 emu/g with zero H_c. In the same study, the nanoparticles obtained with the ultrasonic method showed almost twice as high M_s value (79 emu/g), however, there were H_c values up to 19 Oe. The Fe_3O_4 nanoparticles were synthesized by changing iron salts in [29]. In the study, the M_s values varying between 46.7 and 86.6 emu/g were obtained, however, all samples showed H_c values (8.8–97.5 Oe), and Fe_3O_4 nanoparticles obtained with the highest M_s (86.6 emu/g) had a quite high H_c value of 66.0 Oe. In study [34], M_s of iron oxide nanoparticles was seen to increase from 20 to 68 emu/g with the increase in alkali concentration, and the samples showed $H_c < 5$ Oe. The maximum M_s found in the study is compatible with the value obtained in our study, however, there was H_c (lower than 5 Oe), and the size distribution of the sample showing the best M_s was quite wide according to the TEM analysis. The average particle size was found to be 16 nm, with the sizes ranging from 3 to 57 nm [34]. The iron oxide nanoparticles that were developed for magnetic ink in [6] showed M_s values of 51–53 emu/g without H_c at room temperature. In another study [47], PEGylated Fe_3O_4 nanoparticles were obtained with a two-step synthesis, and superparamagnetic naked Fe_3O_4 nanoparticles obtained in the first step showed a relatively high M_s value of 61 emu/g. Also, in [48], PEG-coated Fe_3O_4 nanoparticles were obtained by in-situ co-precipitation, and uncoated Fe_3O_4 nanoparticles obtained in the study showed M_s value of 80.23 emu/g and H_c value of 14.71 Oe.

In the present study, iron oxide nanoparticles with a significantly high M_s value (67.9 emu/g) and zero H_c were obtained. These nanoparticles may contribute to applications that need superparamagnetic nanoparticles with high M_s, such as magnetic separation, water purification, biosensor applications, and drug delivery. The investigation of the synthesis parameters and obtaining SPIONs with high M_s values may give the opportunity to synthesize the required nanoparticles with controlled synthesis and use them in applications as uncoated nanoparticles or as a core in coated/functionalized nanoparticles.

4. Conclusions

Due to their specific structural and size-dependent characteristics, magnetic nanoparticles are very important for research and development in a variety of fields, including electronics, medicine, and environment. The unique structural, electrical, and magnetic characteristics of iron oxide have garnered a lot of interest recently. In the present study, co-precipitation was used to synthesize SPIONs in an inert atmosphere. The reaction temperature and alkali concentration were adjusted in order to examine the effects of reaction parameters and to obtain SPIONs with high M_s. The reaction temperature was varied between 30 and 90°C, and diluted alkali solutions with different concentrations, from 2.6 to 13.3 M, were used. Structural characterizations were made by using XRD and FTIR. TEM was used for the determination of particle shapes and sizes. The magnetic properties of the nanoparticles were investigated using VSM. It is determined from the XRD patterns and TEM images that the particle size of SPIONs increases with the increase in reaction temperature. The particle size d_{TEM} of T30 and T75 is 6.2 ± 1.2 and 10.1 ± 2.2 nm, respectively. The value of M_s of the SPIONs also increases from 54.0 to 67.9 emu/g with the increase in reaction temperature from 30 to 75°C. The rise in M_s may be caused by the structural changes as well as the increase in particle size. The particle size d_{TEM} of the SPIONs synthesized using different alkali concentrations is 10.1 ± 2.2 and 8.8 ± 2.5 nm for S13.3 and S5.3, respectively. The histogram of S5.3 shows a slightly bimodal size distribution. Alkali concentration also has an effect on M_s, as the values are between 64.6 and 67.9 emu/g. The highest M_s with a moderate size distribution was obtained for the sample synthesized at 75°C and 13.3 M alkali concentration in our experimental conditions. The effects of reaction parameters of co-precipitation under an inert atmosphere have been presented. SPIONs with high M_s values were obtained for possible applications in many fields, specifically, the fields that require high M_s, such as magnetic separation, water treatment, biosensors, and gene and drug delivery.

Acknowledgments

This work was supported by Balikesir University Research Grant no. BAP 2023/010. The authors would like to thank the State Planning Organization, Turkey, under Grant no 2005K120170, for the VSM system. The authors also thank the Physics Department, Balikesir University, Turkey, for FTIR measurements and the National Nanotechnology Research Center (UNAM), Bilkent University, for XRD and TEM measurements.

References

[1] T. Girardet, P. Venturini, H. Martinez, J.-C. Dupin, F. Cleymand, S. Fleutot, *Appl. Sci.* **12**, 8127 (2022).

[2] G.F. Stiufiuc, R.I. Stiufiuc, *Appl. Sci.* **14**, 1623 (2024).

[3] J.R. Vargas-Ortiz, C. Gonzalez, K. Esquivel, *Processes* **10**, 2282 (2022).

[4] B. Rezaei, P. Yari, S.M. Sanders, H. Wang, V.K. Chugh, S. Liang, S. Mostufa, K. Xu, J.-P. Wang, J. Goěmez-Pastora, K. Wu, *Small* **20**, 2304848 (2024).

[5] R. Wirecka, M.M. Marzec, M. Marciszko-Wiackowska, M. Lis, M. Gajewska, E. Trynkiewicz, D. Lachowicz, A. Bernasik, *J. Mater. Chem. C* **9**, 10453 (2021).

[6] M. Vaseem, F.A. Ghaffar, M.F. Farooqui, A. Shamim, *Adv. Mater. Technol.* **3**, 1700242 (2018).

[7] I.V. Martynenko, D. Kusić, F. Weigert et al., *Anal. Chem.* **91**, 12661 (2019).

[8] A. Hashim, I.R. Agool, K.J. Kadhim, *J. Mater. Sci. Mater. Electron.* **29**, 10369 (2018).

[9] P. Bartko, M. Rajňák, R. Cimbala, I. Kolcunová, K. Paulovičová, M. Timko, P. Kopčanský, J. Kurimský, *Acta Phys. Pol. A* **137**, 970 (2020).

[10] W. Wu, M. Jia, Z. Zhang, X. Chen, Q. Zhang, W. Zhang, P. Li, L. Chen, *Ecotoxicol. Environ. Saf.* **175**, 243 (2019).

[11] L. Zhang, Y. Zhang, Y. Tang, X. Li, X. Zhang, C. Li, S. Xu, *Int. J. Environ. Anal. Chem.* **98**, 215 (2018).

[12] Y. Teng, Y. Du, J. Shi, P.W.T. Pong, *Curr. Appl. Phys.* **20**, 320 (2020).

[13] M. Asgari, M. Soleymani, T. Miri, A. Barati, *J. Mol. Liq.* **292**, 111367 (2019).

[14] Z. Hedayatnasab, A. Dabbagh, F. Abnisa, W.M.A.W. Daud, *Eur. Polym. J.* **133**, 109789 (2020).

[15] N. Sanaeifar, M. Rabiee, M. Abdolrahim, M. Tahiri, D. Vashaee, L. Tayebi, *Anal. Biochem.* **519**, 19 (2017).

[16] S.M. Dadfar, D. Camozzi, M. Darguzyte et al., J. *Nanobiotechnol.* **18**, 1 (2020).

[17] K. Kaczmarek, T. Hornowski, R. Bielas, D. Żak, M. Timko, A. Józefczak, *Acta Phys. Pol. A* **133**, 716 (2018).

[18] P. Wu, Z. Xu, *Ind. Eng. Chem. Res.* **44**, 816 (2005).

[19] B.P. Branchaud, *J. Am. Chem. Soc.* **127**, 14117 (2005).

[20] N. Manousi, E. Rosenberg, E. Deliyanni, G.A. Zachariadis, V. Samanidou, *Molecules* **25**, 1148 (2020).

[21] O. Polit, M.S. Shakeri, Z. Swiatkowska-Warkocka, *Acta Phys. Pol. A* **145**, 139 (2024).

[22] M. Islam, A. Rahman, A. Alam, M. Rahman, O.T. Mefford, A. Ul-Hamid, J. Miah, H. Ahmad, *ACS Omega* **9**, 20891 (2024).

[23] S. García-Jimeno, J. Estelrich, *Colloids Surf. A Physicochem. Eng. Aspects* **420**, 74 (2013).

[24] P. Tartaj, in: *Encyclopedia of Nanoscience and Nanotechnology*, Ed. H.S. Nalwa, Vol. 6, American Scientific Publishers, Valencia (CA) 2003.

[25] M. Faraji, Y. Yamini, M. Rezaee, *J. Iran Chem. Soc.* **7**, 130 (2010).

[26] M. Banñobre-López, A. Teijeiro, J. Rivas, *Rep. Pract. Oncol. Radiother.* **18**, 397 (2013).

[27] X. Li, J. Wei, K.E. Aifantis, Y. Fan, Q. Feng, F.Z. Cui, F. Watari, *J. Biomed. Mater. Res. A* **104**, 5 (2016).

[28] S. Laurent, D. Forge, M. Port, A. Roch, C. Robic, L. Vander Elst, R.N. Muller, *Chem. Rev.* **108**, 2064 (2008).

[29] H. Iida, K. Takayanagi, T. Nakanishi, T. Osaka, *J. Colloid Interface Sci.* **314**, 274 (2007).

[30] W. Wu, Q. He, C. Jiang, *Nanoscale Res. Lett.* **3**, 397 (2008).

[31] K. Durak, M. Wiertel, Z. Surowiec, A. Miaskowski, *Acta Phys. Pol. A* **132**, 1593 (2017).

[32] N. Abu Yazid, Y.C. Joon, *AIP Conf. Proc.* **2124**, 020019 (2019).

[33] L. Babes, B. Denizot, G. Tanguy, J.J. Le Jeune, P. Jallet, *J. Colloid Interface Sci.* **212**, 474 (1999).

[34] G. Perez, M.P. Romero, E.B. Saitovitch, F.J. Litterst, J.F.D.F. Araujo, D.C. Bell, G. Solorzano, *Solid State Sci.* **106**, 106295 (2020).

[35] A.S. Omelyanchik, K.V. Sobolev, N.R. Shilov, N.V. Andreev, M.V. Gorshenkov, V.V. Rodionova, *Nanobiotechnol. Rep.* **18**, 879 (2023).

[36] H. Mohammadi, E. Nekobahr, J. Akhtari, M. Saeedi, J. Akbari, F. Fathi, *Toxicol. Rep.* **8**, 331 (2021).

[37] M.M. Khowdiary, H. Alsnani, M.S.A. Darwish, *Inorganics* **12**, 47 (2024).

[38] I. Khmara, M. Kubovcikova, M. Koneracka et al., *Acta Phys. Pol. A* **133**, 704 (2018).

[39] R. Massart, *IEEE Trans. Magn.* **17**, 1247 (1981).

[40] B.D. Cullity, S.R. Stock, *Elements of X-Ray Diffraction*, 3rd Ed. Pearson Prentice Hall, New Jersey 2001.

[41] D. Maity, D.C. Agrawal, *J. Magn. Magn. Mater.* **308**, 46 (2007).

[42] R.M. Cornell, U. Schertmann, *The Iron Oxides: Structure, Properties, Reactions, Occurrence and Uses*, VCH Publishers, Weinheim 2003.

[43] R.F. Ziolo, E.P. Giannelis, B.A. Weinstein, M.P. O'Horo, B.N. Ganguly, V. Mehrotra, M.W. Russell, D.R. Huffman, *Science* **257**, 219 (1992).

[44] L. Zhang, G.C. Papaefthymiou, J.Y. Ying, *J. Appl. Phys.* **81**, 6892 (1997).

[45] C.P. Hunt, M.B. Moskowitz, S.K. Banerjee, *Magnetic Properties of Rocks and Minerals, Rock Physics and Phase Relations: A Handbook of Physical Constants*, Vol. 3, American Geophysical Union, Washington DC 1995.

[46] Z.L. Liu, H.B. Wang, Q.H. Lu, G.H. Du, L. Peng, Y.Q. Du, S.M. Zhang, K.L. Yao, *J. Magn. Magn. Mater.* **283**, 258 (2004).

[47] F. Abrinaei, M. Naseroleslami, *Opt. Laser Technol.* **106**, 327 (2018).

[48] M.F. Tai, C.W. Lai, S.B.A. Hamid, *J. Nanomater.* **2016**, 8612505 (2016).